Visible-Light Activation of H_2O_2 by Red-Mud/Biochar: $^1O_2$ Pathway for Efficient Tetracycline Degradation

Yi Han [a, b, c], Ting Shi [a], Shuai Yang [b], Mingming Wu [a], Hongcheng Gao [a], Dejin Wang [a, c], Emeka E. Oguzie [d], Changyong Zhang [b*]

a College of Resources and Environment, Anqing Normal University, Anqing 246011, China

b Department of Environmental Science and Engineering, University of Science and Technology of China, Hefei 230026, China

c Key Laboratory of Aqueous Environment Protection and Pollution Control of Yangtze River of Anhui Provincial Education Department, Anqing 246011, China

d Africa Centre of Excellence in Future Energies and Electrochemical Systems (ACE-FUELS), Federal University of Technology Owerri, PMB 1526 Owerri, Imo State, Nigeria

*Corresponding Author. E-mail address: changyongzhang@ustc.edu.cn

Catalog

Texts

Tables

Table. S1. Main chemical composition of RM and SCG.

Table. S2. Elemental analysis of SCG.

Table. S3. N_2 adsorption-desorption isotherms of parameters of RM and RMSCG70.

Figures

Fig. S1. The results of phase identification and quantification for RMSCG Biochar Sample (a) RMSCG10, (b) RMSCG30, (C) RMSCG50, (d) RMSCG70, (e) RMSCG90 (The bottom curve indicated the difference, and the vertical bars indicated the Bragg reflection position of the corresponding phases).

Fig. S2. Nitrogen adsorption-desorption isotherms and pore structure of RMSCG70.

Fig. S3. EDS report.

Fig. S4. Hysteresis curves of RMSCG70.

Fig. S5. (a) CV curves of RM, SCG, RMSCG10, RMSCG70, (b) EIS curves of RM, SCG, RMSCG10, RMSCG70.

Fig. S6. Tauc plots of RM and RMSCG70.

Fig. S7. Mott–Schottky curves of RM and RMSCG70.

Fig. S8. (a) $^{\bullet}OH$ fluorescence intensity in light, (b) in dark.

Fig. S9. $O_2^{\bullet-}$ concentration in light and dark.

Fig. S10. (a) XPS profiles of Fe 2p before and after degradation, (b) Process changes of Fe^{2+}/Fe^{3+}.

Fig. S11. The degradation effect of leachate on TCH.

Fig. S12. XRD spectra catalytic and 1st use catalyst.

Fig. S13. H_2O_2 concentration under different systems.

Fig. S14. Different pollutants removal.

Fig. S15. MS spectrum of TCH degradation products.

Fig. S16. Assessment of acute and chronic toxicity of TCH and its intermediates via ECOSAR.

Texts

Text S1. Chemicals

Tetracycline hydrochloride (TCH, ≥ 99.5%) was purchased from Aladdin Chemical Company in Shanghai, China. The main chemical compositions of the red mud and spent coffee grounds determined by X-ray fluorescence (XRF) analysis are shown in Table. S1. Sodium chloride (NaCl), sodium bicarbonate ($NaHCO_3$), sodium sulfate (Na_2SO_4), tert-butanol (TBA), $FeSO_4$-$7H_2O$ (≥ 99.5%), and H_2O_2 (30 wt%) were purchased from Sinopharm Chemical Reagent Co., Ltd. (Shanghai, China). L-Histidine (L-His), p-Benzoquinone (p-BQ), potassium iodide (KI), 1-Butanol, Oxytetracycline Hydrochloride (OTC), Chlortetracycline Hydrochloride (CHC), Doxorubicin Hydrochloride Nitrotetrazolium (DOX), Methylene blue (MB), Rhodamine B (RhB), Blue chloride (NBT), 1,3-Diphenylisobenzofuran (DPBF), and terephthalic acid (PTA) were purchased from Macklin Biochemistry Co., LTD. (Shanghai, China). Ultrapure water was prepared using the UP-SMART system (18.25 MΩ·cm, ULUPURE). All chemicals used were of analytical grade and used without further purification.

Text S2. Characterization methods

The concentration of TCH was determined by an ultraviolet spectrophotometer (Shimadzu UV-2600). The morphology of RMSCG was employed by scanning electron microscope (SEM, JEOL-7800, Japan). The structure of the sample was analyzed by Hitachi Dhammax-IIIA X-ray diffractometer (XRD). A vibrating sample magnetometer (VSM, Lake Shore7404, USA) was used to determine the material magnetism. The surface properties and pore sizes of RMSCG were estimated by nitrogen adsorption-desorption experiment (BET, JW-BK122W, China). The samples were characterized and analyzed by X-ray photoelectron spectroscopy (XPS, Thermo Kalpha, USA).

The organic functional groups on the surfaces of biochars were determined using a Fourier transform infrared spectrometer (FTIR, Thermo Scientific IS5, USA) in the wavelength range of 4000-400 cm^{-1}. The carbon structure of the material before and after the reaction was analyzed using Raman spectroscopy (Raman, Horiba LabRAM HR Evolution, Japanese). Total organic carbon (TOC) was measured using a Jena Multi N/C 3100 (Germany). The formed active radicals were identified by electron paramagnetic resonance (EPR, Bruker A300, America) using DMPO (5,5-dimethyl-1-pyrroline-N-oxide) and TEMP (2,2,6,6-tetramethylpiperidine) as a probe. The Ecological Structure Activity Relationship (ECOSAR v2.2) was used to predict the acute toxicity of the target compound to fish, Daphnia magna and green algae. The average visible light intensity was ca. 106 mW cm^{-2} measured by the photometer (PM100). In the continuous flow reactor, with a reactor volume of 250 mL (85 mm × 40 mm × 140mm) and the same light intensity (106 mW cm^{-2}) were used. Based on different hydraulic residence times, the flow rates were 0.384, 0.461, 0.576, 0.768, and 1.152 L/h, respectively (peristaltic pump, Leardfluid, BT100S). The concentration of Fe^{2+} was detected by the 1,10-Phenanthroline spectrophotometric method. The H_2O_2 content in the solution was measured at a wavelength of 400 nm using the potassium titanium oxalate method. The production of $^{\bullet}OH$ was monitored by the terephthalic acid method. $O_2^{\bullet-}$, $^1O_2$ was quantified by 1,3-diphenylisobenzofuran (DPBF) and nitroblue tetrazolium (NBT) as probe reagents, respectively.

Text S3. Analytical method of H_2O_2

To determine the concentration of H_2O_2, a UV spectrophotometer was used for testing. Take 1 mL of the filtered solution into a cuvette, add 1.6 mL of H_2SO_4 (3 mol/L) and 1.6 mL of $C_4H_2K_2O_{10}Ti$ (0.05 mol/L) and dilute to 10 mL, shake quickly and leave for 10 minutes to ensure complete reaction. The absorbance was measured at 400 nm.

Text S4. Analytical method of $^{\bullet}OH$

Instead of TCH solution, 0.5 mmol of terephthalic acid solution was prepared with 2.0 mmol/L NaOH solution and the rest of the conditions were the same. The solution was removed at certain time intervals and filtered. Then the fluorescence intensity in the range of 400-600 nm was measured by fluorescence spectrometer at 315 nm excitation wavelength (Li et al., 2023).

Text S5. Analytical method of $O_2^{\bullet-}$

The TCH solution was replaced with a 20 mg/L NBT solution and the rest of the conditions were the same. The solution was removed at regular intervals and filtered. Then 1 ml of the solution was diluted to 5 ml and the absorbance was measured at 259 nm (Yu et al., 2024). The $O_2^{\bullet-}$ concentration was then determined from the reduction of NBT using Eq.1.

$$\left\{2.0 - \left[\left(\frac{A_t}{A_0}\right) \times 2.0\right] \times \frac{5}{817.64}\right\} \times 4 \times 1000\ (\mu mol) \quad (1)$$

where 2.0 is the NBT mass (mg); A_0 and A_t are the absorbance of NBT solution at 0 and t min, respectively; 5 is the dilution factor (1–5 mL); 817.64 is NBT molar mass (g/mol); 4 is the stoichiometric factor between reaction of $O_2^{\bullet-}$ and NBT; 1000 is the conversion factor from mmol to μmol.

Text S6. Analytical method of $^1O_2$

The molar ratio of $^1O_2$ to DPBF is 1:1.19. The concentration of $^1O_2$ can be obtained by measuring the concentration of DPBF. 100 μL of the solution was added to 20 mL of DPBF ethanol solution. After 4 hours in the dark, the absorbance of the clarified solution was measured at 410 nm (Zhu et al., 2024).

Text S7. Analytical method of TCH oxidation products

The products of tetracycline hydrochloride (TCH) were analyzed using a high-performance liquid

chromatography-mass spectrometry (HPLC–MS) system manufactured by Agilent Technologies. An automatic sampler was used to inject 5 μL of the sample into a BEH C18 column (2.1 × 100 mm, 1.7 μm), with a flow rate of 0.3 mL/min. The gradient elution program is set to 30°C. The mobile phase consisted of a 0.1% formic acid aqueous solution and methanol solution. Mass spectrometry data were analyzed in positive ion mode (ESI^+) using a molecular ion scanning mode, with a mass range of 100-1100 m/z.

Tables

Table. S1. Main chemical composition of RM and SCG.

Constituents	CaO (%)	MgO (%)	SiO_2 (%)	Fe_2O_3 (%)	Al_2O_3 (%)	MnO_2 (%)
RM	0.960	0.170	15.330	36.210	25.210	0.030
SCG	16.171	6.065	5.673	1.124	0.872	/

Table. S2. Elemental analysis of SCG.

Sample	N (%)	C (%)	H (%)	S (%)	O (%)
SCG	2.18	51.08	7.06	0.12	/

Table. S3. N_2 adsorption-desorption isotherms of parameters of RM and RMSCG70.

Sample	BET surface area (m^2/g)	Pore Volume (cm^3/g)	Pore Size (nm)
RM	13.912	1.216	3.495
RMSCG70	147.470	1.712	4.642

Figures

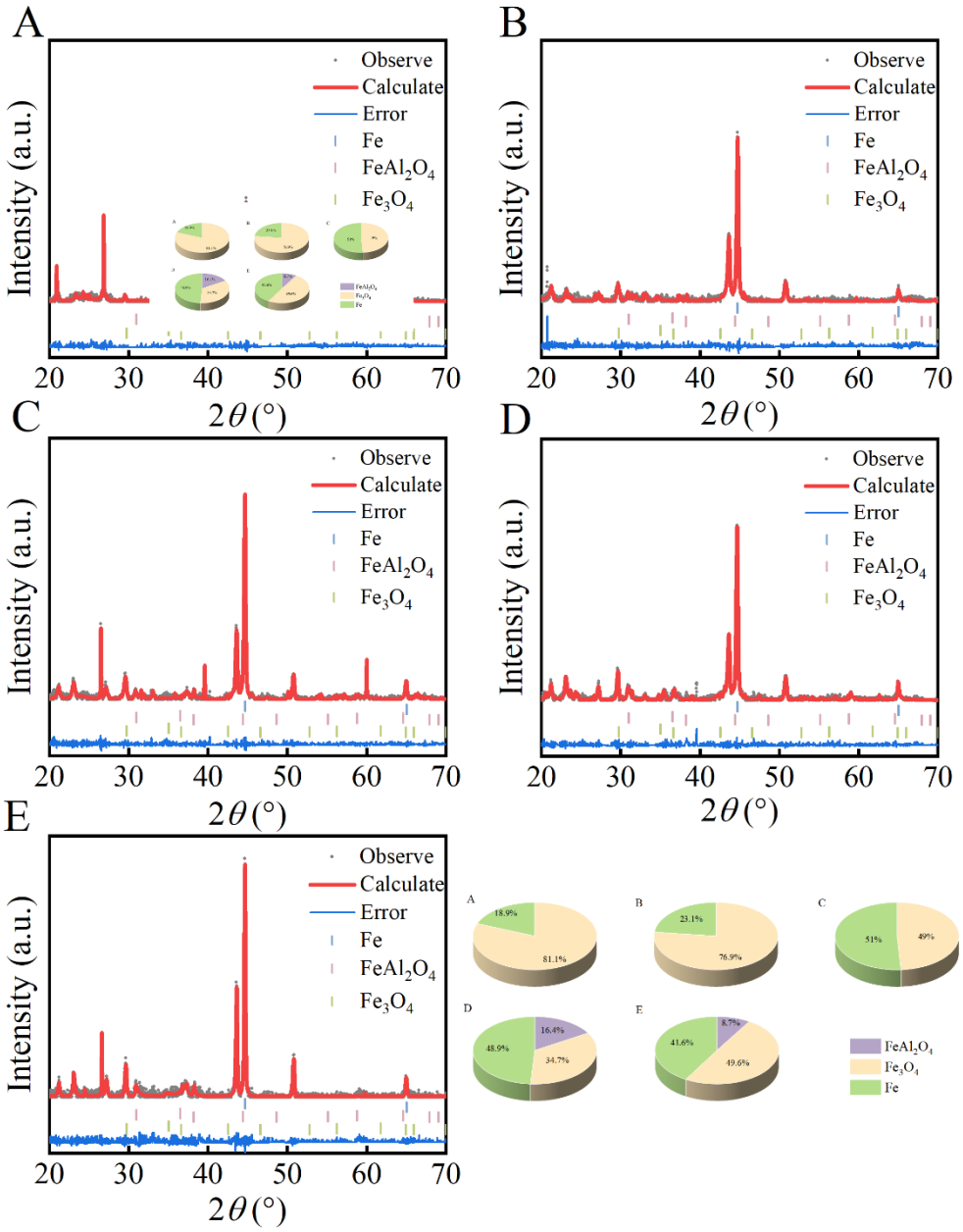

Fig. S1. The results of phase identification and quantification for RMSCG Biochar Sample (a) RMSCG10, (b) RMSCG30, (C) RMSCG50, (d) RMSCG70, (e) RMSCG90 (The bottom curve indicated the difference, and the vertical bars indicated the Bragg reflection position of the corresponding phases).

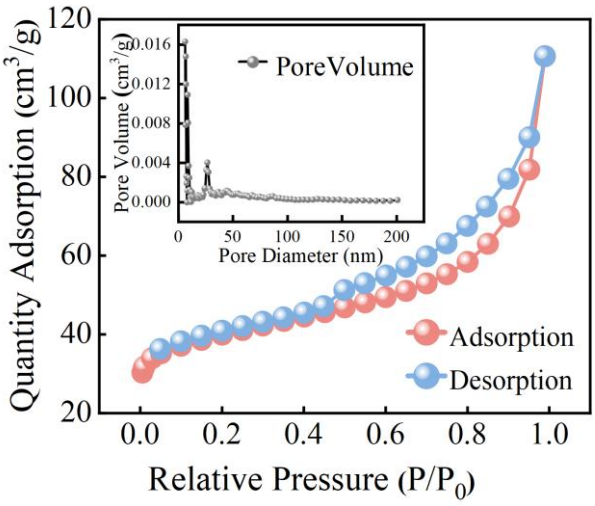

Fig. S2. Nitrogen adsorption-desorption isotherms and pore structure of RMSCG70.

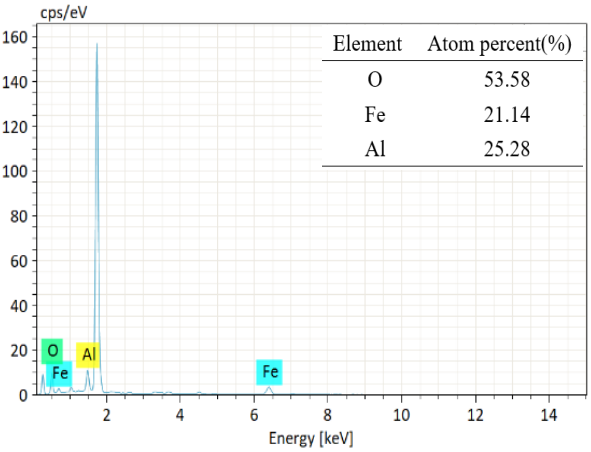

Element	Atom percent(%)
O	53.58
Fe	21.14
Al	25.28

Fig. S3. EDS report.

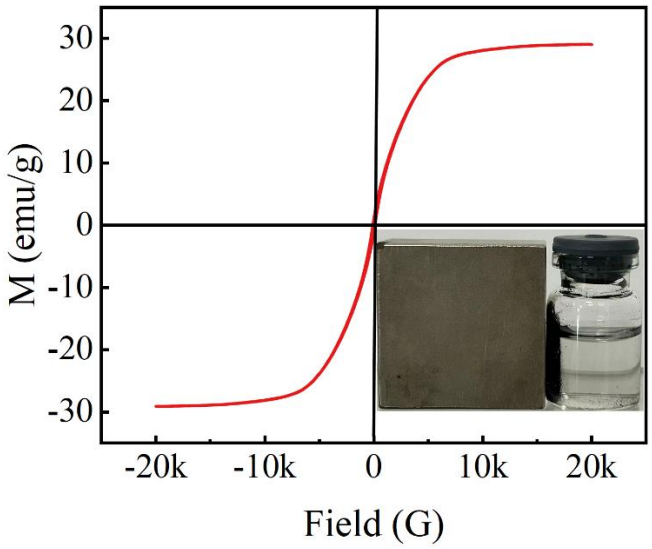

Fig. S4. Hysteresis curves of RMSCG70.

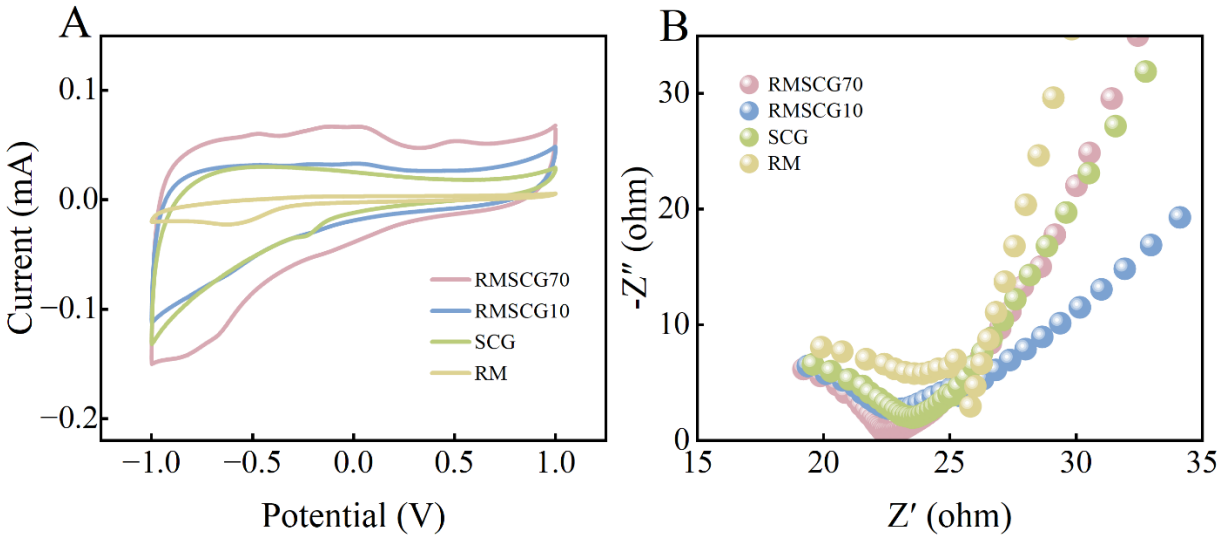

Fig. S5. (a) CV curves of RM, SCG, RMSCG10, RMSCG70, (b) EIS curves of RM, SCG, RMSCG10, RMSCG70.

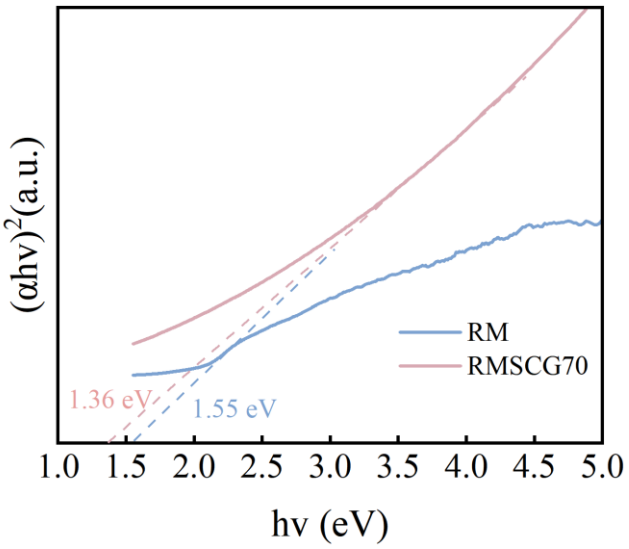

Fig. S6. Tauc plots of RM and RMSCG70.

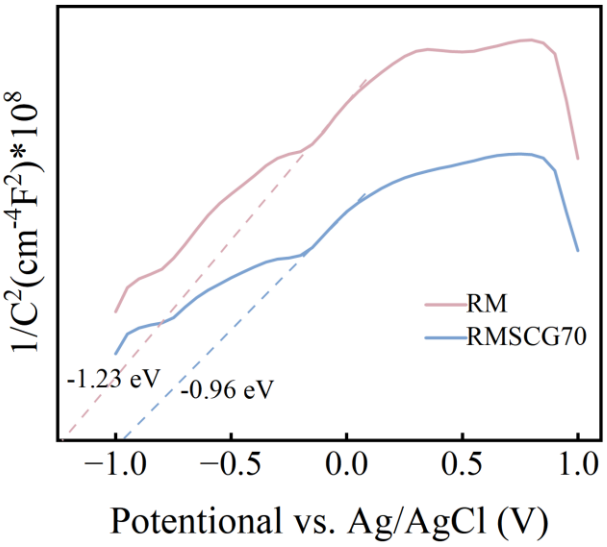

Fig. S7. Mott–Schottky curves of RM and RMSCG70.

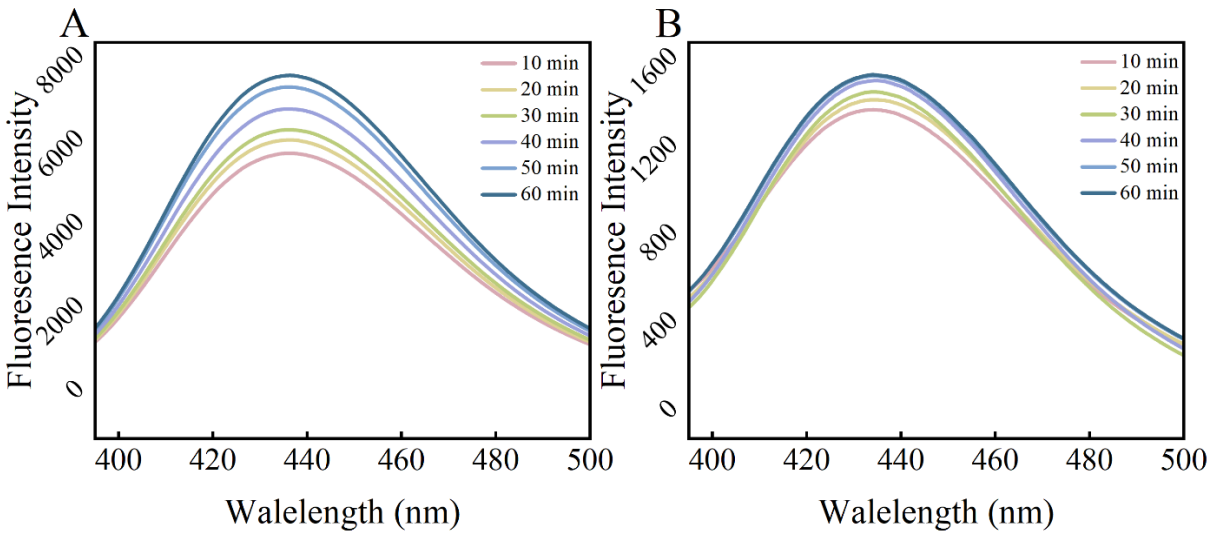

Fig. S8. (a) $^{\bullet}$OH fluorescence intensity in light, (b) in dark.

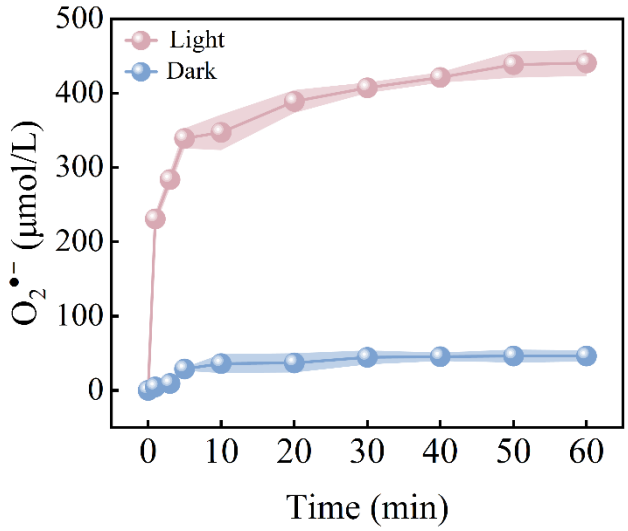

Fig. S9. $O_2^{\bullet-}$ concentration in light and dark.

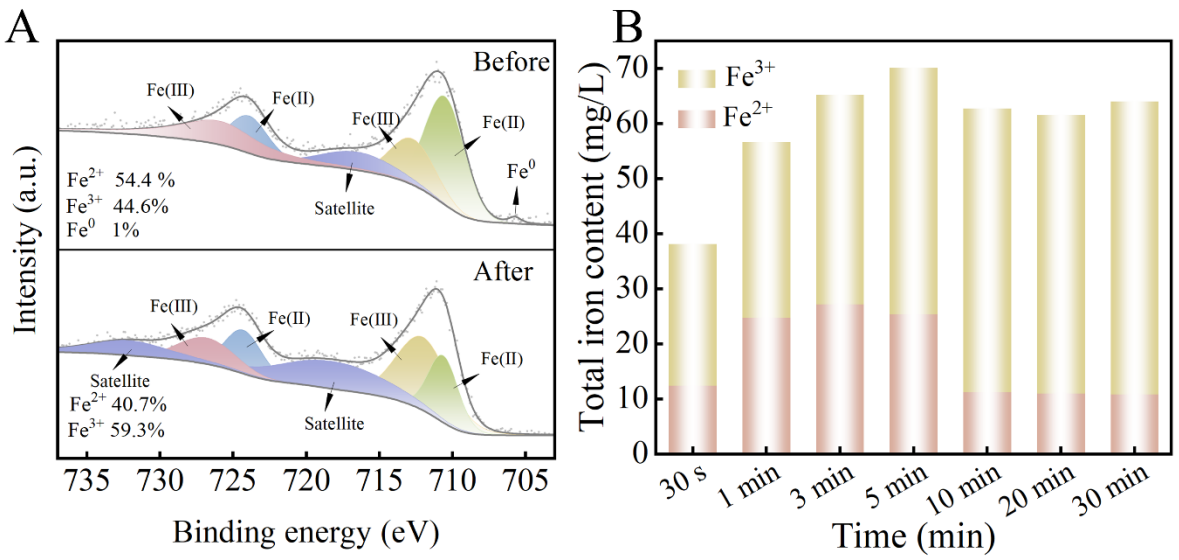

Fig. S10. (a) XPS profiles of Fe 2p before and after degradation, (b) Process changes of Fe^{2+}/Fe^{3+}.

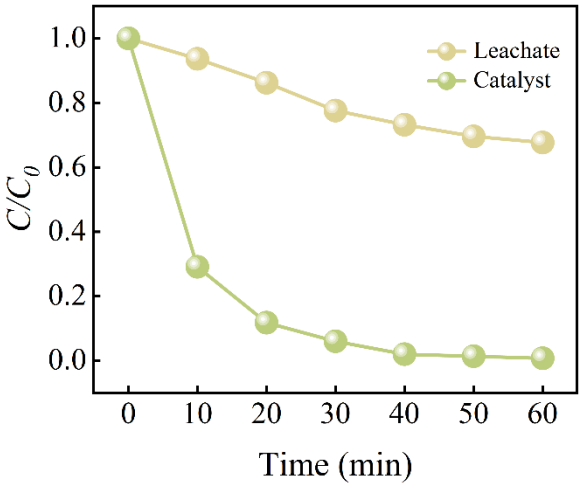

Fig. S11. The degradation effect of leachate on TCH.

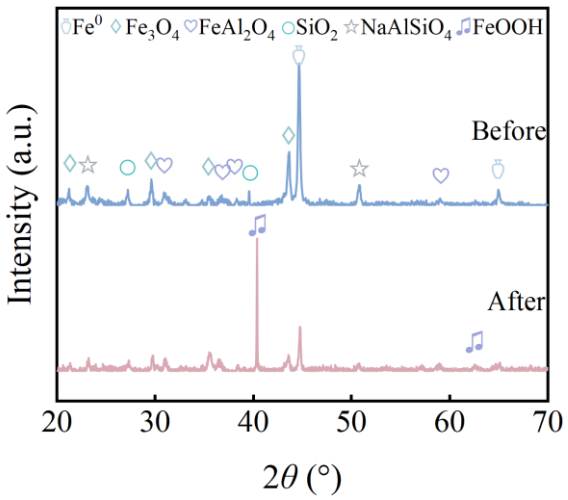

Fig. S12. XRD spectra catalytic and 1st use catalyst.

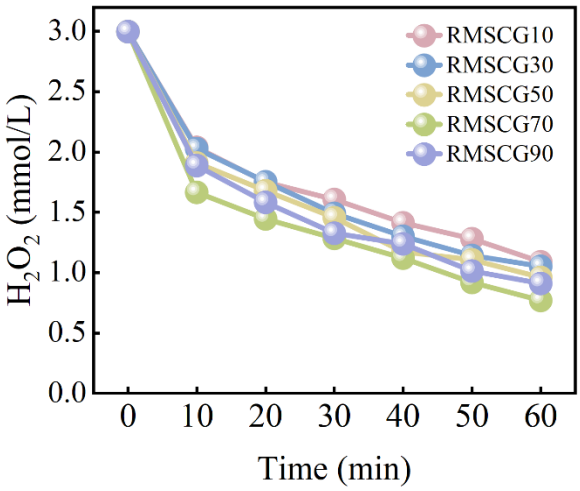

Fig. S13. H_2O_2 concentration under different systems.

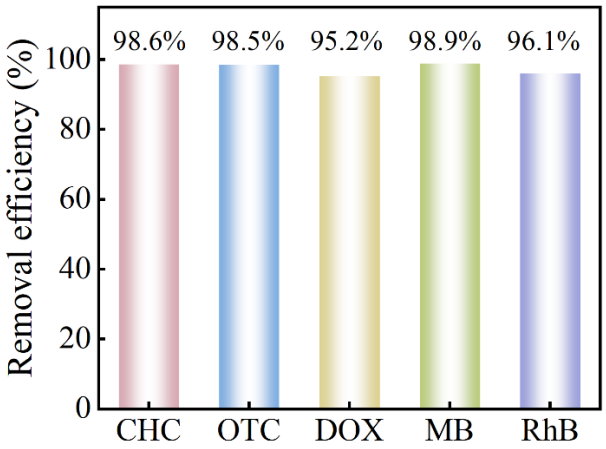

Fig. S14. Different pollutants removal.

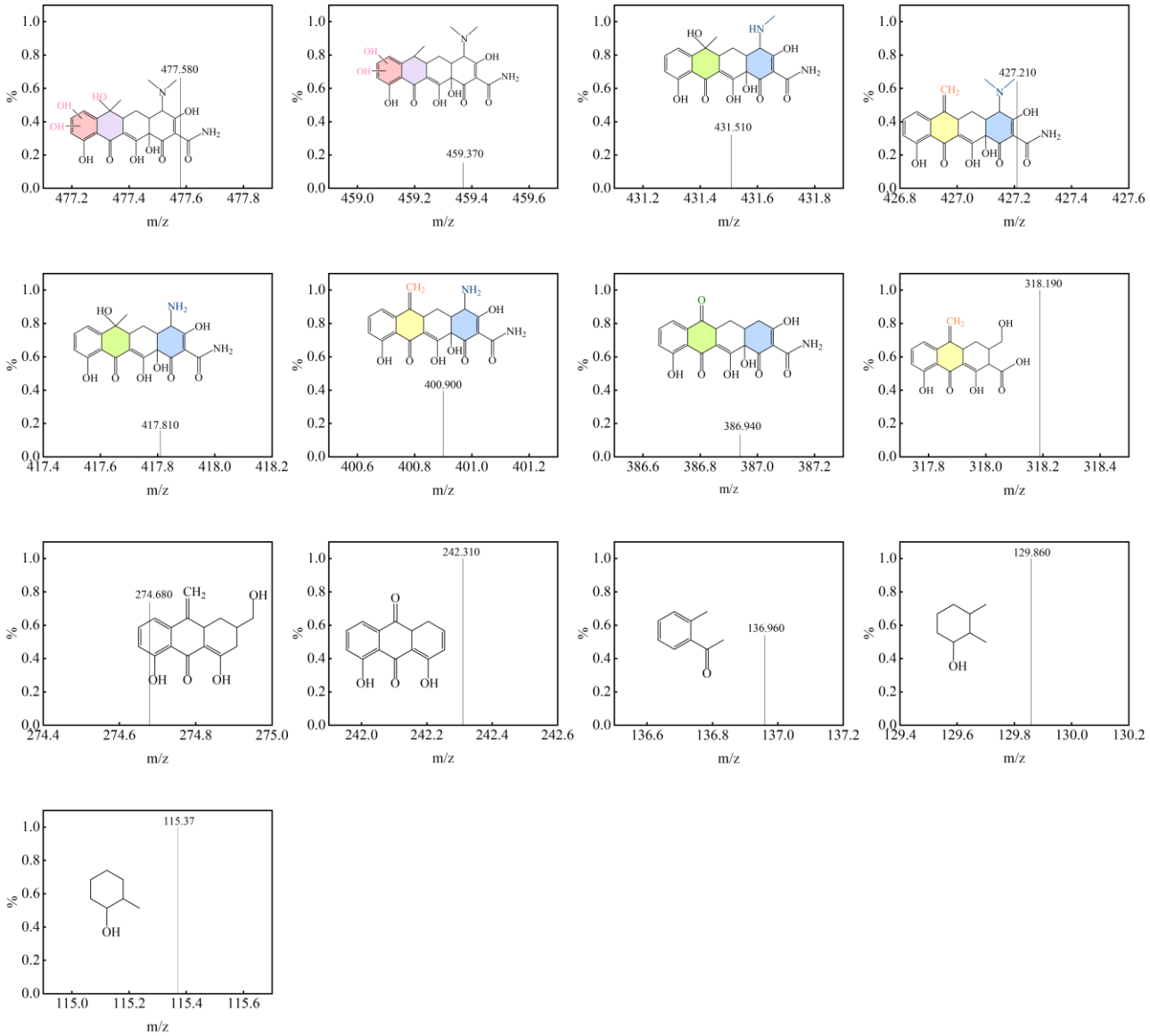

Fig. S15. MS spectrum of TCH degradation products.

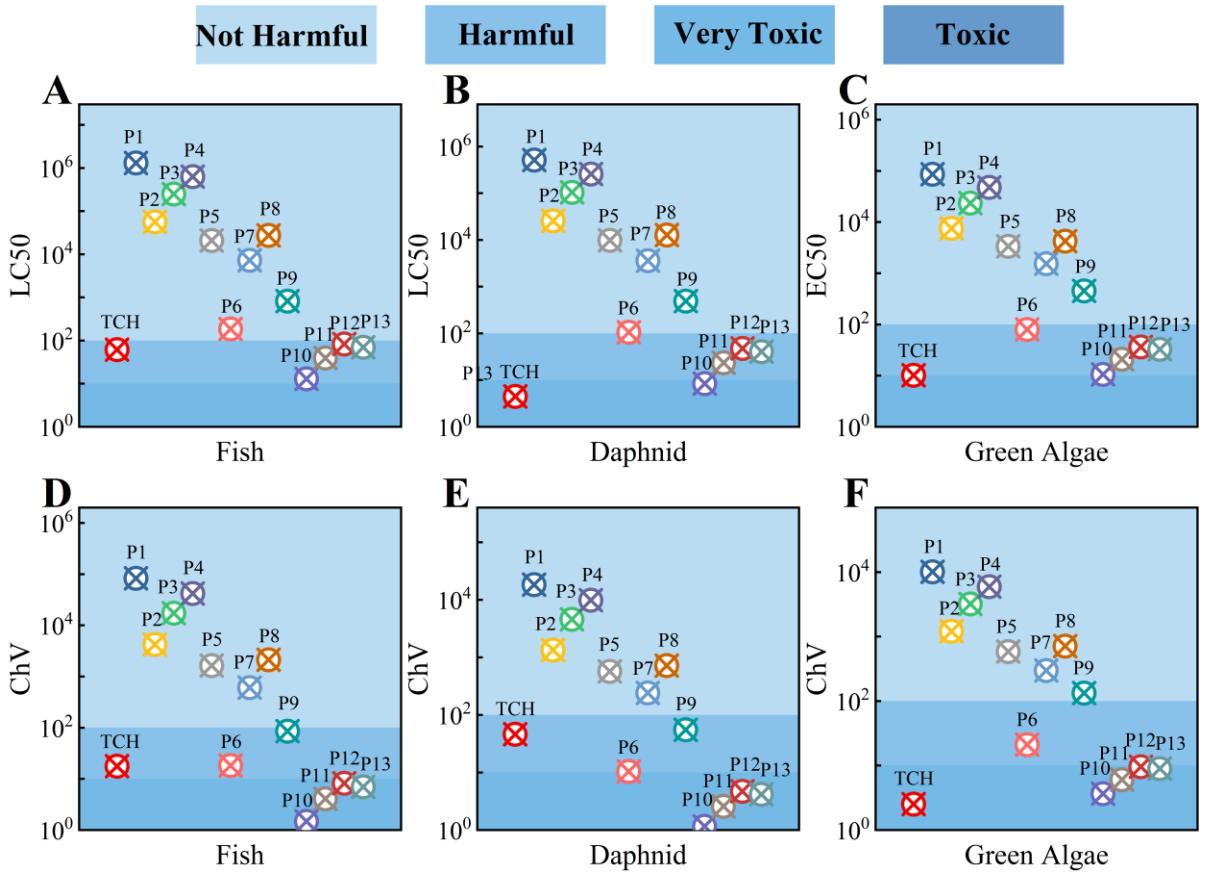

Fig. S16. Assessment of acute and chronic toxicity of TCH and its intermediates via ECOSAR.

References

Li Y, Yu B, Li H, Liu B, Yu X, Zhang K, Qin G, Lu J, Zhang L, Wang L (2023). Activation of hydrogen peroxide by molybdenum disulfide as Fenton-like catalyst and cocatalyst: Phase-dependent catalytic performance and degradation mechanism. Chinese Chemical Letters, 34(5): 107874

Yu C, Guo C, Zhang Y, Gu J, Shi M, Wan J, Wang L, Pan J (2024). Hitting two birds with one stone: A ce-modified Fe-based bi-functional material reinforced fenton-like system for complete removal of organophosphorus pesticides. Chemical Engineering Journal, 497: 154828

Zhu G, Fan X, Yu Y, Liu Y, Quan X (2024). Regulating the Electronic Structure of Cu Single-Atom Catalysts toward Enhanced Electro-Fenton Degradation of Organic Contaminants via $^1O_2$ and •OH. Environmental Science & Technology, 58(43): 19545-19554